Geophys. Astrophys. Fluid Dynamics, Vol. 43. pp. 1–41
Reprints available directly from the publisher
Photocopying permitted by license only

Printed in Great Britain

Critical-Layer Absorption of Neutral Ageostrophic Vorticity Wave Perturbations of Baroclinic Jets

GORDON E. SWATERS

Applied Mathematics Institute, Department of Mathematics, University of Alberta, Edmonton, Alberta T6G 2C6, Canada

(*Received 8 October 1987; in final form 12 January 1988*)

A theory is presented which describes the along-front propagation and cross-front trapping, due to the absorption by multiple critical-layers, of ageostrophic non-divergent perturbations of baroclinic jets. The perturbations are dispersive neutral vorticity waves which use the jet vorticity gradient as a pseudo-β effect.

The wave streamfunction and temperature anomaly take the form of horizontally tilted "cat's eyes doublets" which propagate in the direction of jet flow, but which have relatively large retrograde group velocities. Between the critical-layers, the wave-induced transverse Reynolds stress acts to transfer momentum (and heat) from the warm side critical-level to the cool side critical-level of the jet. There is no *net* wave-mean flow energy transfer. Exterior to the region containing the critical-levels the Reynolds stress is zero. The ageostrophic component of the wave field acts to shift the node in the wave-induced temperature anomaly toward the warm side of the jet. The wave streamfunction exterior to the region containing the critical-levels is obtained by asymptotically matching solutions valid in the exterior "near-fields" of the critical levels to WKB solutions valid far from the jet. In between the critical-levels, the wave streamfunction is obtained in the form of an infinite spectral series of spheroidal wave functions. The solutions for the two regions are patched together by requiring the normal mass flux and reduced pressure to be bounded and continuous. The dispersion relation for the vorticity waves is written in the form of an infinite continued fraction.

KEY WORDS: Baroclinic jets, critical layer absorption, cross-front trapping, cat's eyes.

1. INTRODUCTION

Near-inertial *internal* waves have been observed to contribute a significant fraction of the velocity finestructure associated with fronts. For example, Kunze and Sanford (1984) analyzed current and XBT measurements of the North Pacific Subtropical Front collected during the *FRONTS'80* experiment (Niiler, 1982; *EOS Transactions*, 1980) and showed that about 75% of the velocity finestructure is contained in near-inertial internal waves. Similar observations have been made for other fronts, for example, by Mayer *et al.* (1979) on the Mid-Atlantic Shelf. However, in addition to providing a waveguide for internal waves, the usually large vorticity gradients associated with frontal currents may locally dominate the planetary vorticity gradient providing a local pseudo-β effect allowing along-front propagation of relatively low-frequency neutral baroclinic *vorticity* waves. The principle purpose of this paper is to present a simple analytical theory describing the along-front propagation and cross-front trapping due to critical layer absorption of these "frontal-vorticity" waves.

The theoretical study presented in this paper was motivated by an "anomalous" cross-front XBT temperature profile (see Figure 1) of the North Pacific Subtropical Front (NPSF) observed on January 25 during *FRONTS'80* (Kunze, 1985, private communication), briefly described but not published in Kunze and Sanford (1984). (It should

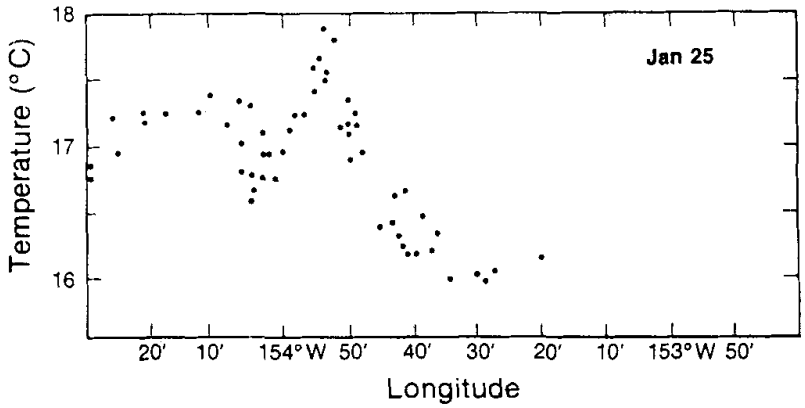

Figure 1 Transverse temperature section derived from XBT data taken from the North Pacific Subtropical Front during *FRONTS'80* depicting a transient warm–cold temperature core pair. The values have been averaged over 100–150 m and represent deflections of the base of the mixed layer.

be emphasized at this point, however, that the theory described in this paper is general and should not be considered as simply an attempt to "model" Figure 1. The following description of Figure 1 should be understood as motivational and not exhaustive or complete.) The temperature profile, shown in Figure 1, shows a transient warm–cold core pair. Although Kunze and Sanford (1984) did not directly measure the displacement of the base of the mixed layer, the temperature feature was only present between 100 and 150 m (the mixed layer depth was between 110–130 m) and Kunze (private communication, 1985) has interpreted Figure 1 as the result of vertical displacements of the base of the mixed layer. The warm–cold core pair appeared in only one of six sections taken across the NPSF [see Kunze and Sanford (1984) Figure 3 for a more typical temperature structure]. The period between sections was about 12 hours. The temperature dipole was therefore interpreted as having short time scales and/or short along-front length scales.

However, the cross-front length scales seemed too large for the warm–cold core pair to be interpreted as an internal-gravity wave. Kunze and Sanford (1984) argued that the internal wave spectrum during *FRONTS'80* was dominated by horizontal scales on the order of $O(10)$ km. Assuming a trough-to-peak distance that is about one-half a wavelength, the temperature dipole in Figure 1 has a cross-front length scale $O(15–20)$ km, which is similar to the frontal transverse length scale.

Kunze and Sanford (1984) also pointed out that the temperature dipole in Figure 1 was displaced to the warm side (i.e. synoptically to the south) of the NPSF. As a rough estimate, the node of the warm-cold core pair in Figure 1 is displaced approximately 20′–30′ (longitude) or about 20–25 km in the direction of the warm side of the front.

The internal waves observed in *FRONTS'80* current and XBT data were strongly modulated by the geostrophic vorticity associated with the NPSF current. Kunze and Sanford (1984) computed an effective Coriolis frequency including the effects of the relative vorticity of the NPSF current. In the cross-front direction, the frontal vorticity resulted in about a 10% variability in the effective Coriolis frequency. Near the axis of symmetry in the NPSF current, the frontal vorticity *gradient* was predominately constant (Kunze and Sanford, 1984) and dominated the planetary vorticity gradient.

Kunze and Sanford (1984) [see also Roden (1981)] suggest an *e*-folding cross-front decay scale of about 10–15 km and current magnitude of 10–20 cms^{-1}, hence the ratio of the planetary vorticity gradient to the geostrophic vorticity shear is about $O(\beta L^2/U_*) \sim 10^{-2}$. Thus in the immediate region adjacent to the frontal axis of symmetry the ambient geostrophic vorticity gradient can dominate the planetary vorticity gradient and provide a local pseudo-β effect allowing the propagation of along-front neutral *vorticity* waves (called frontal-vorticity waves).

Analytical studies of wave perturbations of geostrophic jets are relatively few in number because the cross-front (or transverse) structure of the perturbations must, in general, satisfy a non-constant coefficient Rayleigh stability equation [e.g. (3.20a)] and exact solutions to this equation are difficult to obtain. A typical *ansatz* has been to model flows with piecewise constant velocity profiles (e.g. the rectangular or top hat jet) or piecewise linear velocity profiles (e.g. the symmetric trapezium jet). The solutions for these and other similar zero vorticity gradient jet profiles can be found in Drazin and Howard (1966).

The *Bickley* jet (Savic, 1941; see also Drazin and Howard, 1966) has been used to study various aspects of the instability mechanism for continuous jets with nonzero vorticity gradient, since for this profile the Rayleigh stability equation can be transformed into a Legendre equation. For example, Stern (1961) used the Bickley jet profile to examine the effect of small horizontal mass divergences in the instability of baroclinic jets. Lipps (1962, 1963) made similar investigations.

However, these studies have been formulated within the quasi-geostrophic approximation. As mentioned previously, there is a significant ageostrophic component to the velocity finestructure associated with fronts. This peak in the velocity spectrum cannot be explained entirely in terms of wind-generated inertial oscillations (Stern, 1977).

It will be shown in this paper that many of the qualitative features of Figure 1 are consistent with the predictions of a vorticity wave critical-level interaction theory. The geostrophic component of the wave amplitude will be shown to contain a single node in the cross-front direction. The ageostrophic component of the cross-front wave amplitude acts to shift the apparent cross-front temperature node

associated with the vorticity wave toward the warm side of the front (as suggested by the NPSF data). The along-front length and time scales inferred from the data (see Section 3) suggest that the perturbations are horizontally nondivergent but contain an important ageostrophic component.

The waves described here will have phases which propagate in the direction of the jet flow. However, the inviscid group velocities are found to be relatively large [$O(2\text{–}3\,\mathrm{ms}^{-1})$], and are retrograde with respect to the jet. (This property is exactly analogous to the propagation of *high* meridional wavenumber planetary Rossby waves in a constant zonal flow). Consequently, an along-front time scale based on the group velocity will be relatively short. For the NPSF application a typical estimate for the wavelength/Döppler-shifted group velocity is about seven hours (see Section 5). Also, the along-front length-scale is on the same order as the transverse shear in the jet velocity profile. (Both are about one-half the internal deformation radius for the *FRONTS'80* region, see Section 2.)

It is important to add that the anomalous XBT section shown in Figure 1 could equally well be interpreted as an intrusion, inversion, isolated small scale meander, a sloping front, or in terms of baroclinic and barotropic instability, etc. Indeed, it is likely that the *origin* of the warm–cold core pair is the result of one of these mechanisms. In this context, the theory presented here provides a mechanism for the rapid along-front propagation of a perturbation of a jet, once the anomaly has formed. With regard to this latter possibility it is interesting to note that Roden (1981) observed significant thermal inversions as a result of a storm passing through the *FRONTS'80* experimental site. Shortly after the storm had subsided, Roden (1981) observed that the temperature inversions were no longer present and speculated, on the basis of energy arguments, that along-front motions were responsible.

A detailed comparison between the theory developed in this paper and the anomalous XBT section shown in Figure 1 is inappropriate because the data represents a single isolated observation, so a detailed time series describing the along-front evolution of the warm–cold temperature pair is not available. The point of view adopted here is to simply regard the interesting event shown in Figure 1 as the physical motivation for developing the theory described in this paper, and to show that the generic predictions of

the theory are not inconsistent with the qualitative interpretation given to Figure 1.

The plan of the paper is as follows. In Section 2 the relevant synoptic features of the NPSF jet which motivated the model used in this study are briefly reviewed. In Section 3, the governing non-dimensional equations of the model are given. Based on parameter estimates determined in Section 2, the basic model assumed are the non-linear reduced-gravity equations on a f-plane.

In Section 4 the model equations are solved. Section 4.1 describes the wave solutions exterior to the critical levels. In Section 4.2 the wave solutions between the critical levels is obtained under the approximation that the separation distance between the critical levels is small compared to the shear in the jet velocity profile.

The general solution for the wave streamfunction, in the region between the critical levels, is a linear combination of a function which is analytic at *both* critical levels and a second function which has (removable) logarithmic singularities at *both* critical levels. Both functions are obtained as spectral series expansions in spheroidal wave functions. The dispersion relation is obtained as a result of determining the analytic solution, and is written in the form of an infinite continued fraction.

In Section 5 the properties of the solution are described and a qualitative application to the NPSF is made. Section 6 summarizes the paper.

2. BRIEF SYNOPSIS OF THE NPSF CURRENT

The mesoscale features of the North Pacific Subtropical Front and the associated baroclinic current have been fully described in Roden (1981) and Kunze and Sanford (1984). Drifter data and SST's for the *FRONTS'80* region derived from satellite data is described in Van Woert (1982). In this section the objective is to simply highlight the relevant NPSF current features which moticated the model formulation developed in this paper.

The North Pacific Subtropical Front separates the relatively cool and dense central North Pacific water from the relatively warm and

less dense southern North Pacific water. Roden and Paskauski (1978) have suggested that the origin of the NPSF is governed by the geographic variability in solar heating and wind stress. The NPSF, which is centred roughly along 30 °N over most of the Pacific basin, has an accompanying eastward-flowing surface intensified baroclinic jet. At the surface the NPSF current has a magnitude of about 20 cm/s and at a depth of 100 m the magnitude is about 10 cm/s. Below the mixed layer the current rapidly decays with depth (Roden, 1981). During the time the XBT data shown in Figure 1 was taken, the depth of the mixed layer was between 110–130 m [Kunze (1985) private communication; note that Figure 1 contains data averaged over 100–150 m]. The NPSF jet is symmetrical about the front with an *e*-folding length scale of about 10–15 km (Kunze and Sanford, 1984). Kunze and Sanford (1984) modelled the cross-front structure of the NPSF current with a Gaussian function and this is the geostrophic jet model adopted in this paper.

During *FRONTS'80* the NPSF was distorted from a simple zonal configuration into a convolution with a "wavelength" and "amplitude" of about 200 km and 100 km, respectively (Kunze and Sanford, 1984). Satellite buoy tracks (Roden, 1981, Figure 9) indicate that to the east of the convolution the circulation was cyclonic and to the west anticyclonic. Perhaps this long wavelength distortion [compared to the internal deformation radius for the *FRONTS'80* experimental region, which is about 37.5 km (Emery *et al.*, 1984)] is an example of a long-wave instability as described by Killworth (1983).

Roden (1981) computed cross-front profiles of the vertical structure of, among other variables, temperature (see Roden's Figure 11). Keeping in mind that the temperatures in Figure 1 have been averaged over about 100–150 m, the warm core in Figure 1 of approximately 17.75 °C corresponds to water at about 115 m depth and the cold core in Figure 1 of approximately 16.25 °C corresponds to a depth of 140 m [as an average between the profiles shown in Roden (1981)]. The 17°C mark, which is interpreted as the "undisturbed" water temperature, corresponds to a depth of about 125 m (which is about the depth of the base of the mixed layer). Therefore, as a crude first estimate, the vertical displacements in Figure 1 associated with the warm cold core pair on the order of ± 10 m in about 125 m of water.

3. FORMULATION OF THE MODEL

Since the NPSF current is a surface intensified and horizontally strongly sheared jet (Roden, 1981; Kunze and Sanford, 1984), the basic model assumed will be the nonlinear reduced-gravity equations on a f-plane, which can be written (LeBlond and Mysak, 1978, Section 16) in the dimensional form

$$u^*_{t^*} + u^* u^*_{x^*} + v^* u^*_{y^*} - f v^* + g' h^*_{x^*} = 0, \tag{3.1}$$

$$v^*_{t^*} + u^* v^*_{x^*} + v^* v^*_{y^*} + f u^* + g' h^*_{y^*} = 0, \tag{3.2}$$

$$h^*_{t^*} + [u^*(H + h^*)]_{x^*} + [v^*(H + h^*)]_{y^*} = 0, \tag{3.3}$$

with f, g' and h^* the constant Coriolis parameter, the reduced gravity $(\rho_2 - \rho_1)g/\rho_1$ and the mixed layer *thickness* deviation, respectively (see Figure 2). Derivatives are denoted by subscripts. The

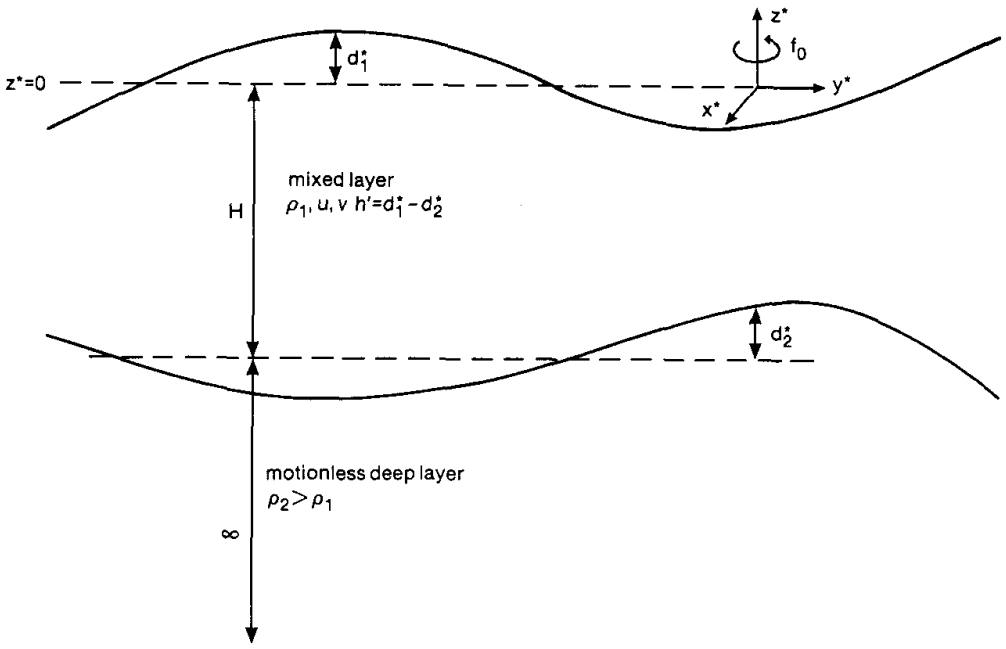

Figure 2 Geometry of the reduced-gravity model used in this paper.

mean depth of the mixed layer is denoted $H \simeq 125\,\mathrm{m}$. The reason for working with the mixed layer thickness deviation rather than the deflection of the base of the mixed layer is that the former is positively correlated with temperature anomalies, whereas the latter is negatively correlated (assuming that baroclinic motions dominate barotropic motions). The velocity components u^* and v^* are the along-front and cross-front components, respectively, and x^* and y^* are the along-front and cross-front (transverse) coordinates, respectively. Substitution of

$$u^* = U_0^*(y^*) + u'(x^*, y^*, t^*), \tag{3.4}$$

$$v^* = v'(x^*, y^*, t^*), \tag{3.5}$$

$$h^* = h_0^*(y^*) + h'(x^*, y^*, t^*), \tag{3.6}$$

where $U_0^*(y^*)$ and $h_0^*(y^*)$ is the NPSF geostrophic jet model of Kunze and Sanford (1984) given by

$$U_0^*(y^*) = U_* \exp(-\alpha_*^2 y^{*2}), \quad U_0^*(y^*) = -g' f^{-1} h_{0_{y^*}}^*(y^*), \tag{3.7, 3.8}$$

into (3.1)–(3.3) and linearizing about the front yields

$$(\partial_{t^*} + U_0^* \partial_{x^*})u' - (f - U_{0_{y^*}}^*)v' + g' h'_{x^*} = 0, \tag{3.9}$$

$$(\partial_{t^*} + U_0^* \partial_{x^*})v' + f u' + g' h'_{y^*} = 0, \tag{3.10}$$

$$(\partial_{t^*} + U_0^* \partial_{x^*})h' + H(u'_{x^*} + v'_{y^*}) = 0, \tag{3.11}$$

where (u', v') and h' are the wave-induced perturbations in the mixed layer velocity field and mixed layer thickness, respectively (see Figure 2).

The remaining analysis is facilitated by casting (3.9), (3.10) and (3.11) into nondimensional form. The length scale is based on the transverse shear of the NPSF jet. The velocity scale is chosen as a representative jet speed and time is scaled based on the advective time scale. The reduced pressure is scaled geostrophically. Thus the nondimensional (unprimed or unasterisked) variables are defined by

$$\begin{aligned} (x^*, y^*) &= L(x, y), \quad t^* = (L/U_*)t, \\ (u', v') &= U_*(u, v), \quad h' = f L U_* (g')^{-1} h, \end{aligned} \tag{3.12}$$

with $L \equiv (2^{1/2}\alpha_*)^{-1}$. Substitution of (3.12) into (3.9)–(3.11) yields

$$r_0(\partial_t + U_0\,\partial_x)u - (1 - r_0 U_{0_y})v + h_x = 0, \tag{3.13}$$

$$r_0(\partial_t + U_0\,\partial_x)v + u + h_y = 0, \tag{3.14}$$

$$Fr_0(\partial_t + U_0\,\partial_x)h + u_x + v_y = 0, \tag{3.15}$$

where $r_0 = U_*(fL)^{-1}$, $F = (L/R_*)^2$ with $R_* = (g'H)^{1/2}/f$ are the Rossby number, rotational Froude number and internal deformation radius, respectively.

The nondimensional frontal jet is given by

$$U_0(y) = \exp(-y^2/2), \tag{3.16a}$$

with the nondimensional mixed layer thickness perturbation associated with the current given by

$$h_0(y) = -\int_{-\infty}^{y} \exp(-\eta^2/2)\,d\eta = -(\pi/2)^{1/2}[\mathrm{erf}(y/2^{1/2}) + 1], \tag{3.16b}$$

where $\mathrm{erf}(\cdot)$ is the usual error function as defined in Abramowitz and Stegun (1972, Chapter 7).

The *effective* dynamical Coriolis frequency in (3.13) is given by

$$1 - r_0 U_{0_y} = 1 + r_0 y \exp(-y^2/2). \tag{3.16c}$$

Thus in the neighborhood of $y = 0$, the effective rotation frequency experienced by a displaced fluid particle is an approximately linear function of the transverse coordinate.

Kunze and Sanford (1984) estimate $U_* \sim 20\,\mathrm{cm/s}$ and an e-folding distance (α_*^{-1}) of about 15 km for the frontal current implying $L \sim 10.6\,\mathrm{km}$. The center latitude of the *FRONTS'80* experimental site was about 30.4 °N yielding $f \sim 7.38 \cdot 10^{-5}\,\mathrm{s}^{-1}$ ($\beta \sim 1.97 \cdot 10^{-11}\,\mathrm{m}^{-1}\,\mathrm{s}^{-1}$). Hence the inertial period is about 23 hours. In order to estimate the rotational Froude number, an estimate of the internal deformation radius is required. Emery *et al.* (1984) calculate an internal deformation radius in this region of

about $R_* \sim 37.5\,\text{km}$. Thus $r_0 \sim 0.25$ and $F \sim 0.1$, implying $Fr_0 \sim 2.5 \times 10^{-2}$. Consequently, for these synoptic parameter values, the flow is essentially horizontally non-divergent, though ageostrophic since the Rossby number is relatively $O(1)$. The effect of neglecting the $O(Fr_0)$ term in (3.15) is to filter out the long internal-gravity (Poincaré) waves and to focus on the ageostrophic vorticity wave solutions to the model. Note that the jet-vorticity gradient locally (i.e. $y \sim 0$) dominates the planetary vorticity gradient with this scaling since $O(\beta y^*/U^*_{0y^*}) \sim \beta L^2/U_* \sim 1.5 \times 10^{-2}$.

Neglecting the $O(Fr_0)$ term in (3.15) and introducing a perturbation streamfunction ϕ into (3.13)–(3.15) yields

$$(u, v) = (-\phi_y, \phi_x), \quad h_x = (1 - r_0 U_{0_y})\phi_x + r_0(\partial_t + U_0\,\partial_x)\phi_y, \quad \text{(3.17a, b)}$$

with ϕ governed by the f-plane vorticity equation

$$(\partial_t + U_0\,\partial_x)\Delta\phi - U_{0_{yy}}\phi_x = 0, \tag{3.18}$$

where $\Delta = \partial^2_{xx} + \partial^2_{yy}$.

Substituting an along-front propagating solution into (3.17) and (3.18) of the forms

$$\phi = \text{Real}\{\phi'(y)\exp(ikx - i\omega t)\}, \tag{3.19a}$$

$$h = \text{Real}\{h'(y)\exp(ikx - i\omega t)\}, \tag{3.19b}$$

where k and ω are the along-front wavenumber and frequency, respectively, results in the f-plane Rayleigh stability equation for the transverse amplitude function $\phi'(y)$ which can be written in the form

$$[c\exp(y^2/2) - 1][\phi_{yy} - k^2\phi] + (y^2 - 1)\phi = 0, \tag{3.20a}$$

where c is the phase speed ω/k (the primes have been dropped). The transverse structure of the wave-induced perturbation to the mixed layer thickness will be ageostrophically determined and given by [cf. (3.19b)]

$$h(y) = (1 - r_0 U_{0_y})\phi + r_0(U_0 - c)\phi_y. \tag{3.20b}$$

The boundary conditions on the solution to the Rayleigh stability equation (3.20a) are that the reduced pressure $h(y)$ and transverse velocity $\phi(y)$ be bounded and continuous functions of y.

It is a corollary of Howard's semi-circle theorem for neutral modes (i.e. c is real) (Drazin and Howard, 1966; Maslowe, 1985) that c lie in the range of $U_0(y)$; i.e., $0<c<1$. Therefore, the neutral wave solutions that are described in this paper will always contain symmetrically placed (about $y=0$) critical levels at $y=\pm y_c(y_c>0)$ where y_c is given by

$$y_c=[-2\ln(c)]^{1/2} \tag{3.21}$$

As $c\to+1^-(U_{\max})$ or $c\to 0^+(U_{\min})$, it follows that $y_c\to 0^+$ or $+\infty$, respectively.

It turns out that all the neutral modes found were evanescent for $|y|>y_c$ [see (4.3) for the necessary and sufficient condition which ensures this]. [Note that (3.20a) implies that as $|y|\to\infty$, $\phi(y)\sim\exp(-k|y|)$.] Thus, in the transverse direction, the wave-like region is $-y_c<y<y_c$. Comparing Figure 1 with more typical cross-NPSF XBT temperature sections in Kunze and Sanford (1984) suggests that $y_c\lesssim 1$ because the peak-to-trough distance in Figure 1 is on the order of the length scale imposed by e-folding shear in the jet. Under the asymptotic limit $0<y_c\ll 1$ or, equivalently, $e^{-1/2}\ll c<1$ substantial analytical progress and physical insight can be made in describing the neutral vorticity wave solutions to (3.20a), and this is the approximation exploited in this paper.

It should also be noted here that the concept of wave over-reflection, which is useful in explaining barotropic and baroclinic critical layer instabilities (e.g. Lindzen and Tung, 1978; Lindzen *et al.*, 1980) does not seem to have a direct application here because the neutral wave modes presented here are evanescent for $|y|>y_c$; i.e. there is no exterior wave source necessary for over-reflection (Lindzen and Tung, 1978).

4. SOLUTION FOR THE TRANSVERSE AMPLITUDE AND DERIVATION OF THE DISPERSION RELATION

In this section an approximate asymptotic solution to (3.20a) is

obtained when $0 < y_c \ll 1$, i.e. the distance from the jet axis of symmetry to the critical levels is small compared to the horizontal *e*-folding shear in the jet. This approximation is consistent with interpreting the warm–cold temperature pair in Figure 1 as having a non-negligible ageostrophic component to it.

Under the above approximation, it will be shown that the Rayleigh stability equation (3.20a) is, including first order wavenumber contributions, a generalized spheroidal wave equation in the *interior* region $-y_c < y < y_c$. Because the indicial equation in the neighborhood of each critical-level has roots 0 and 1, there exists one linearly independent solution to (3.20a) which is analytic at *both* $y = \pm y_c$ and another linearly independent solution to (3.20a) which is logarithmically singular at *both* $y = \pm y_c$. The dispersion relation is obtained from constructing the analytic solution.

The procedure developed here to obtain the perturbation streamfunction and wave dispersion relationship is a novel extension of the usual procedure of constructing a Frobenius expansion about a single critical point (e.g. Pedlosky, 1987, Section 7.8) to the case of two separate critical points. The wave streamfunction, in between the critical levels, is obtained in the form of an infinte series of appropriate basis functions. The procedure developed in this paper to obtain the wave streamfunction, as a spectral series, has been used by various authors to study wave propagation in distorted background flows, for example Lorenz (1972), Gill (1974), Duffy (1975) and Clarke (1975).

In the *exterior* region $|y| > y_c$ there are two sub-regions of interest. Near (but exterior) to the critical levels ($y \sim +y_c^+$ and $y \sim -y_c^-$, respectively), the singular behaviour in (3.20a) dominates and the streamfunction is approximately given by modified Bessel functions. Far from the critical levels ($|y| \gg y_c$) the streamfunction can be approximated with a WKB solution. The near-exterior and far-exterior solutions are asymptotically matched together and a uniformly valid exterior solution is given. The interior and exterior solutions are patched together by requiring the reduced pressure and normal velocity to be continuous across the critical layers. The along-front velocity is found to be logarithmically singular across the critical layers (see Figure 6). At the critical levels the inviscid solution presented here is, of course, no longer valid and additional physics is required, for example friction or nonlinearity.

4.1 Solution for the regions exterior to the critical levels

In this subsection the solutions for $\phi(y)$ and $h(y)$ in the regions $|y|>y_c$ will be obtained. An approximate solution is constructed by asymptotically matching WKB solutions valid far from the critical levels (i.e. $|y|\gg y_c$) to leading order singular solutions valid near but still exterior to the critical levels (i.e. $y\sim y_c^+$ and $y\sim -y_c^-$, respectively). This procedure has been used, for example, by Lindzen and Rosenthal (1981) [see also Lindzen *et al.* (1980)] to obtain quantitatively accurate approximations to the Charney baroclinic instability problem and by Dickinson (1968) to describe critical layer absorption of planetary Rossby waves.

The subsequent analysis in this subsection is facilitated by rewriting the Rayleigh stability equation (3.20a) in the form

$$\phi_{yy}-p(y)\phi=0, \tag{4.1a}$$

where

$$p(y)=k^2+(1-y^2)[c\exp(y^2/2)-1]^{-1}. \tag{4.1b}$$

It is easily shown that $p(y)\to+\infty$ as $y\to -y_c^-$ or y_c^+ provided $c>e^{-1/2}$ or equivalently $y_c<1$. Moreover, it will be shown in Section 4.2 that the allowed phase speeds and wavenumbers obtained from dispersion relation for the frontal-vorticity waves have the property that there are no turning points [i.e. y values for which $p(y)$ changes sign] in $|y|>y_c$. Thus $p(y)>0$ for $|y|>y_c$.

A condition which ensures that no turning points exist for $|y|>y_c$ can be obtained from (4.1b). It follows from (4.1b) that $p(y)$ will be a minimum at $y=y_m(c)$ where y_m satisfies $dp(y_m)/dy=0$, i.e.

$$c(3-y_m^2)=2\exp(-y_m^2/2). \tag{4.2}$$

It can be shown that there is a solution to (4.2) satisfying $y_c<|y_m|<e^{1/2}$ only if $c>e^{-1/2}$. Thus $p(y)$ is positive definite for $y>y_c$ if $p(y_m)>0$, which can be written in the form [cf. (4.1b) and (4.2)]

$$k^2>3-y_m^2(c). \tag{4.3}$$

All of the neutral waves were found to satisfy (4.3).

The condition that a WKB solution to (4.1a) approximates (to leading order) the exact solution to (3.20a) in $|y| \gg y_c$ is (Morse Feshbach, 1961, Section 9.3)

$$\left|\tfrac{1}{2}p^{-3/2}\,\partial p/\partial y\right| \ll 1 \tag{4.4}$$

when $|y| \gg y_c$. It is straightforward to show that the left-hand side of (4.4) exponentially small for $|y| \gg y_c$.

The bounded WKB solution to (4.1a) in the regions $y > y_c$ and $y < -y_c$ can be written, respectively, in the form (Bender and Orszag, 1978)

$$\phi \sim B^{+}[p(y)]^{-1/4} \exp\left\{-\int_{y_c}^{y} [p(\eta)]^{1/2}\, d\eta\right\}, \qquad y > y_c, \tag{4.5}$$

$$\phi \sim B^{-}[p(y)]^{-1/4} \exp\left\{-\int_{y}^{-y_c} [p(\eta)]^{1/2}\, d\eta\right\}, \qquad y < -y_c. \tag{4.6}$$

These solutions are asymptotically matched to approximate solutions valid for $|y| \sim y_c^{+}$. In these regions the singular behaviour of $p(y)$ dominates. The details for $y \sim -y_c^{-}$ are similar to those for $y \sim y_c^{+}$ thus only the latter are presented.

As $y \to y_c^{+}$ the leading order balance in (4.1a) is

$$\phi_{yy} - v^2(y - y_c)^{-1}\phi \sim 0, \tag{4.7}$$

where $v^2 \equiv (1 - y_c^2)/y_c > 0$ when $y_c < 1$. The bounded (as $y \gg y_c$) solution to (4.7) is (Abramowitz and Stegun, 1970, Chapter 9)

$$\phi \sim A^{+}(y - y_c)^{1/2} K_1[2v(y - y_c)^{1/2}], \tag{4.8}$$

where $K_1[*]$ is the modified Bessel function of the second kind of order one. The relationship between A^{+} and B^{+} is obtained by

asymptotically matching the leading order behaviour of (4.5) as $y \to y_c^+$ and (4.8) as $y - y_c \to +\infty$. The leading term of (4.5) as $y \to y_c^+$ is given by

$$\phi \sim B^+(y-y_c)^{1/4} v^{-1/2} \exp\{-2v(y-y_c)^{1/2}\} \tag{4.9a}$$

and of (4.8) as $y - y_c \to \infty$ is given by (Abramowitz and Stegun, 1970, Chapter 9)

$$\phi \sim A^+(\pi/4v)^{1/2}(y-y_c)^{1/4} \exp\{-2v(y-y_c)^{1/2}\}. \tag{4.9b}$$

In the language of boundary-layer theory (e.g. Bender and Orszag, 1978, Chapter 9), the approximate solutions (4.5) and (4.6) correspond to the leading order *outer* solutions for $\phi(y)$ since $p(y)$ varies "slowly" [i.e. (4.4) is satisfied]. The approximate solutions (4.8) [and (4.10a)] correspond to the leading order *inner* or singular-layer solutions for $\phi(y)$ since when $|y| \sim y_c$, $p(y)$ and hence $\phi(y)$ varies "rapidly". Note that it is possible to identify $Y \equiv v^2(y-y_c)$ as a "boundary-layer" variable in (4.7). Following standard boundary-layer matching procedures (e.g. Bender and Orszag, 1978, Chapter 9), the requirement that the *inner* and *outer* approximate solutions be asymptotically consistent demands that the *form* of the two approximate solutions be identical as one moves back and forth from the outer region to the inner region. Lindzen and Rosenthal (1981) have used a similar matching procedure in their WKB study of the Charney instability problem.

Thus, it follows from (4.9a, b) and the asymptotic matching requirement that

$$B^+ = \pi^{1/2} A^+/2. \tag{4.9c}$$

Similarly, it can be shown that

$$\phi \sim A^- |y+y_c|^{1/2} K_1[2v|y+y_c|^{1/2}] \tag{4.10a}$$

for $y \sim -y_c^-$ and consequently that

$$B^- = \pi^{1/2} A^-/2. \tag{4.10b}$$

The amplitude coefficients A^+ and A^- will be determined (up to a free multiplication constant) by requiring the pressure and normal velocity component to be continuous at $y=\pm y_c$.

The uniformly valid leading order structure of the wave-induced streamfunction for $y>y_c$ is therefore given by (4.8) plus (4.5) minus the "overlap" term (4.9b) with B^+ given by (4.9c). A uniformly valid leading order solution for the region $y<-y_c$ is constructed similarly.

4.2 Solution for the region in between the critical levels and derivation of the dispersion relation

In the region $-y_c<y<y_c$ the condition for the validity of the WKB *ansatz* [i.e. (4.4)] no longer holds and an alternate solution procedure is required. It was argued in Section 3 that Figure 1 suggests that $0<y_c\lesssim 1$. This qualitative observation can be exploited by constructing a solution to (3.20a) formally valid for $0<y_c\ll 1$. To this end a stretched coordinate η, given by

$$y=[2(1-c)/(cy_c^2)]^{1/2}y_c\eta, \tag{4.11}$$

is introduced. The coefficient in the square bracket in (4.1) is $O(1)$ and significantly simplifies the subsequent algebra.

Substitution of (4.11) into the Rayleigh stability equation (3.20a) results in the approximate balance

$$(\eta^2-1)\phi_{\eta\eta}-(\alpha+\beta\eta^2)\phi=0, \tag{4.12}$$

where α and β are parameters given by

$$\alpha=[-2k^2(1-c)+2]/c, \quad \beta=2k^2(1-c)/c. \tag{4.13a, b}$$

In the derivation of (4.12) all terms of order $O[\eta^{2n}(1-c)^n]$ for $n\geqq 2$ have been neglected. This approximation can be formally justified when $0<1-c\ll 1$ and by noting that $0<\eta^2<1$ for the region in between the critical levels. However, the $O(1-c)$ terms in the parameters α and β have been retained because, as it will be shown, they are very important in determining the correct dispersion relationship for the frontal-vorticity waves. Without these two terms no solutions were found for the yet-to-be derived dispersion relation-

ships (4.22). In particular, it is important to note that these two terms will determine the *dispersive* properties of the waves because they are the leading order terms that *explicitly* contain the wavenumber and therefore will determine how the phase speed c varies with k. We believe Eq. (4.12) retains the essential physics in the region $-y_c<y<y_c$, namely; symmetrically placed critical levels and a relatively constant jet vorticity gradient.

Equation (4.12) is a *generalized* spheroidal wave equation (Morse and Feshbach, 1961, Section 5.2) with regular singular points at $\eta=\pm 1$ (the critical level locations). The indicial equation at $\eta=\pm 1$ has roots 0 and 1. Therefore, provided α and β satisfy a to-be-determined eigencondition, there exists one homogeneous solution to (4.12) [denoted $\phi_1(\eta)$] which is analytic in $-1\leqq\eta\leqq 1$ and another linearly independent solution which contains logarithmic branch points at $|\eta|=1$ (Boyce and DiPrima, 1977, Section 4.6).

Near $\eta=+1$ (i.e. $y=+y_c$) and $\eta=-1$ (i.e. $y=-y_c$) the logarithmic solutions will have the respective forms [Drazin and Reid (1981), Section 22; see also Pedlosky (1987), Section 7.8 or LeBlond and Mysak (1978), Section 41]

$$\phi^+\sim\phi_2^+(\eta)+\tfrac{1}{2}(\alpha+\beta)\phi_1^+(\eta)\ln(\eta-1), \tag{4.14a}$$

$$\phi^-\sim\phi_2^-(\eta)-\tfrac{1}{2}(\alpha+\beta)\phi_1^-(\eta)\ln(\eta+1), \tag{4.14b}$$

where ϕ_2^+ and ϕ_2^- are analytic functions at $\eta=+1$ and $\eta=-1$, respectively, and $\phi_1^+\sim O(\eta-1)$ and $\phi_2^+\sim O(\eta+1)$ as $\eta\to+1$ and -1, respectively. Standard arguments (Boyce and DiPrima, 1977, Section 4.6) imply that (4.14a) will have a radius of convergence $-1<\eta<3$ and (4.14b) $-3<\eta<1$. A linear combination of the two will therefore have a radius of convergence $-1<\eta<1$, i.e. the required interior critical level region.

It can be shown that $\phi_1^+(\eta)$ and $\phi_1^-(\eta)$ correspond to the exponentially unbounded solutions in $|y|>y_c$ which were discarded in (4.8) and (4.10a), i.e. the possible $I_1[2\nu(y-y_c)^{1/2}]$ and $I_1[2\nu|y+y_c|^{1/2}]$ solutions.

If one examines the forms suggested by (4.14a, b) for the appropriate $|\eta|\simeq 1$ structure in the logarithmic solutions it seems natural to attempt to construct a complete solution for the entire region $|\eta|<1$

in the form

$$\phi(\eta) \sim \phi_2(\eta) + \tfrac{1}{4}(\alpha+\beta)\phi_1(\eta) \ln [(\eta-1)/(\eta+1)], \qquad (4.14c)$$

where $\phi_2(\eta)$ is analytic in $|\eta| \leqq 1$ and where $\phi_1(\eta)$ is $O[2(\eta+1)]$ and $O[2(\eta-1)]$ as $\eta \to -1$ and $+1$, respectively. It turns out that $\phi_1(\eta)$ is an even function in η about $\eta=0$ and thus the logarithmic term in (4.14c) retains the sign convention suggested in (4.14a, b). A solution of the form (4.14c) is a modest generalization of the usual procedure for obtaining the logarithmic solution in a neighborhood of a single critical level to the case of two separable critical points.

The appropriate branch to take for the multi-valued function $\ln [(\eta-1)/(\eta+1)]$ is determined by the sign of $U_{0_y}(y)$ at $y = \pm y_c$ and the requirement not to cut the real y (or η) axis (in the complex plane) as the neutral mode is approached from slightly unstable modes (Pedlosky, 1987, Section 7.8). Because $U_{0_y}(+y_c) < 0$ and $U_{0_y}(-y_c) > 0$ under the approximation $y_c \ll 1$, the correct vertical branch cuts are *below* and *above* the real η axis at $\eta = +1$ and $\eta = -1$, respectively. Thus the logarithmic term in the solution (4.14c) is defined to take the values

$$\ln [(\eta-1)/(\eta+1)] = \ln [(\eta-1)/(\eta+1)], \quad |\eta| > 1, \qquad (4.14b)$$

$$\ln [(\eta-1)/(\eta+1)] = \ln [(1-\eta)/(\eta+1)] + \pi i, \quad |\eta| < 1. \qquad (4.14c)$$

Consequently, there will be a $+\pi$ and $-\pi$ radian phase shift across the critical levels as η passes through $+1$ and -1 from above, respectively. It will be shown in Section 5 that this phase shift will result in a nonzero constant northward wave-induced Reynolds stress in $|\eta| < 1$ and a zero Reynolds stress in the exterior regions $|\eta| > 1$.

The analytic homogeneous solution $\phi_1(\eta)$ required in (4.14c) is most conveniently expressed [following the methods outlined in Morse and Feshbach (1961, Section 5.2) for generalized spheroidal wave equations] in the form

$$\phi_1(\eta) = (\eta^2 - 1) \sum_{n=0}^{\infty} a_n T_n^{(1)}(\eta), \qquad (4.15)$$

where $T_n^{(1)}(\eta)$ are *Gegenbauer* (or associated Legendre) polynomials

(Morse and Feshbach, 1961, Section 5.2 and Chap. 6) with upper index one. The reader is referred to the above citation for a complete description of the properties of these orthogonal polynomials. However, a list of the properties required for the present study is contained in the Appendix. A solution in the form (4.15) is an example of an infinite spectral series expansion. Similar expansions have been used, for example, by Lorenz (1972) and Gill (1974) in a Rossby wave stability analysis and Dickinson (1968a, 1968b), Clarke (1975) and Niehaus (1980) to study wave propagation in distorted background flows.

Substitution of (4.15) into (4.12) results in [exploiting (A.1)]

$$\sum_{n=0}^{\infty}[2-\alpha+n(n+3)]a_nT_n^{(1)}-\beta\eta^2\sum_{n=0}^{\infty}a_nT_n^{(1)}=0. \tag{4.16}$$

Rewriting $\eta^2T_n^{(1)}$ in terms $T_{n-2}^{(1)}$, $T_n^{(1)}$ and $T_{n+2}^{(1)}$ by applying (A.2) twice and re-arranging the sums results in the three term recurrence relation

$$a_{n+2}+\gamma_na_n+\mu_na_{n-2}=0, \quad n\geqq 0, \tag{4.17a}$$

where

$$\gamma_n=\left[\frac{1-k^2}{k^2}-\frac{cn(n+3)}{2k^2(1-c)}+\frac{(n+1)(n+3)}{(2n+3)(2n+5)}\right.$$
$$\left.+\frac{n(n+2)}{(2n+3)(2n+1)}\right]\frac{(2n+5)(2n+7)}{(n+4)(n+3)}, \tag{4.17b}$$

$$\mu_n=n(n-1)(2n+5)(2n+7)/[(n+4)(n+3)(2n-1)(2n+1)], \tag{4.17c}$$

and it is understood $a_{-2}=a_{-1}\equiv 0$.

In the classification scheme of Tung (1976) the recurrence relation (4.17a) is called *class b* because *both* the coefficients γ_n and μ_n do not approach finite limits as $n\to+\infty$. It follows from (4.17b) and (4.17c) that

$$\gamma_n\sim -2cn^2/k^2(1-c), \quad \mu_n\sim 1, \tag{4.18a, b}$$

for $n\gg 1$. As pointed out in Tung (1976) (see also the references

therein) class b three term recurrence relations have two types of solutions: a rapidly diverging one and a rapidly converging one. The are given asymptotically for large n, respectively, as

$$a^{(1)}_{n+2}/a^{(1)}_n \sim n^2 2c/k^2(1-c), \quad a^{(2)}_{n+2}/a^{(2)}_n \sim k^2(1-c)/2cn^2. \quad (4.19a, b)$$

It is a classical theorem in the calculus of finite difference equations, i.e. *Perron's Theorem* [for example see Milne-Thompson (1933), also Tung (1976)], that the a_n's computed from the recurrence relation (4.17a) will correspond to the rapidly converging solution (4.19b) *if and only if* the determinant of the coefficient matrix associated with (4.17), containing the γ_n's and μ_n's, is zero. [Here, the recurrence relation (4.17) is being thought of as an *infinite* dimensional linear homogeneous system in the a_n's ($n>0$).] The requirement that the coefficient matrix be singular forms the dispersion relationship between the phase speed and wavenumber.

It is important to understand that if the phase speed and wavenumber are not connected in the above manner, the computed a_n's *must* diverge according to (4.19a). But if this were the case, then $\phi_1(\eta)$ would not be bounded because the series in (4.15) would not converge, and if $\phi_1(\eta)$ is not bounded then $\phi(n)$ itself is not bounded and is not analytic *as it must be.* A complete discussion of these methods can be found in Morse and Feshbach (1962, Section 5.2) or Tung (1976).

The condition that the coefficient matrix in (4.17) be singular (i.e. its determinant vanishes) is most easily expressed as a continued fraction [see Tung (1976) and Morse and Feshbach (1961, Section 5.2)]. The recurrence relation (4.17a) can be rearranged into the form

$$a_n/a_{n-2} = -\mu_n/(\gamma_n + a_{n+2}/a_n). \quad (4.20)$$

It also follows from (4.17) that

$$a_2/a_0 = -\gamma_0, \qquad a_3/a_1 = -\gamma_1. \quad (4.21a, b)$$

Thus, by iterating (4.20) and using (4.21a, b) it follows

$$\gamma_0 = \mu_2/\{\gamma_2 - \mu_4/[\gamma_4 - \mu_6/(\ldots\ \ldots)]\}, \quad (4.22a)$$

or

$$\gamma_1 = \mu_3/\{\gamma_3 - \mu_5/[\gamma_5 - \mu_7/(\ldots\ \ldots)]\}, \tag{4.22b}$$

for the even and odd coefficients, respectively. Equations (4.22a) and (4.22b) are the dispersion relationships for the problem.

Equations (4.22) contain an infinite number of terms in the continued fraction. However, from (4.19b) the successive fractions a_{n+2}/a_n will be $O(n^{-2})$ for large n. In practice, therefore, truncating the fraction in (4.22) after a large number of terms will yield a good approximation to the correct dispersion relationship. The dispersion relationships were computed by retaining 600 terms. Additional terms had absolutely no effect on the results to double precision accuracy. It was found that there were *no* c and k values which satisfy the odd dispersion relationship (4.22b). Thus $\phi_1(\eta)$ is composed solely in terms of even functions.

Figures 3a, b and c are graphs of the wavenumber, phase speed and group velocity versus frequency, respectively, found by solving the even dispersion relation (4.22a) for the along-front wavenumber as a function of the phase speed c when $0 < c < 1$. There was a low phase speed cutoff of about 0.21. For all phase speeds greater than the cutoff and bounded above by 1, a unique wavenumber was found.

A cautionary note is required here. Notwithstanding the fact that

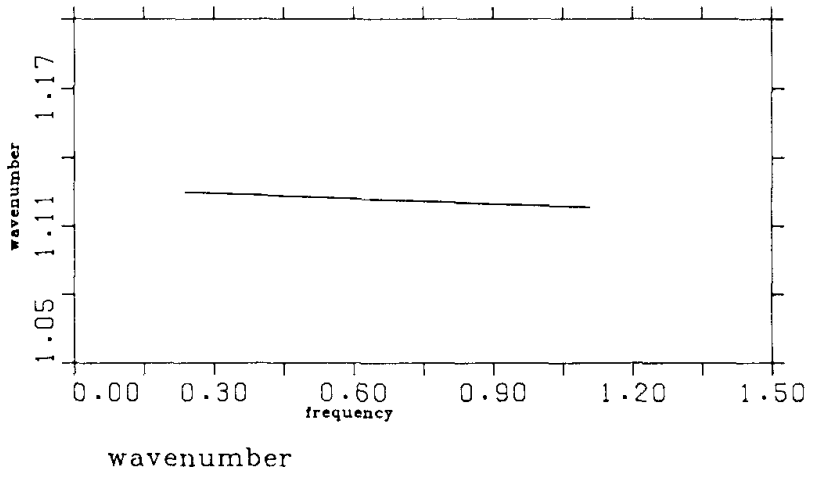

Figure 3(a) The wavenumber/frequency curve obtained from solving the dispersion relation (4.22a). The wavenumber is a slightly super-linear function of the frequency.

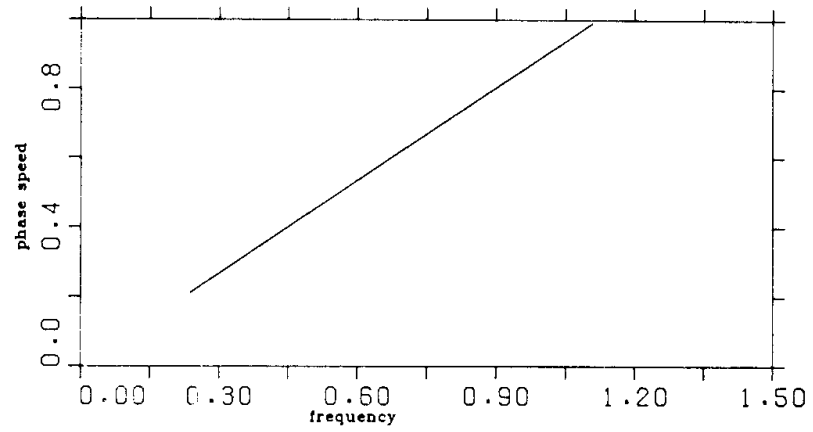

Figure 3(b) The phase speed/frequency curve obtained from the dispersion relation (4.22a).

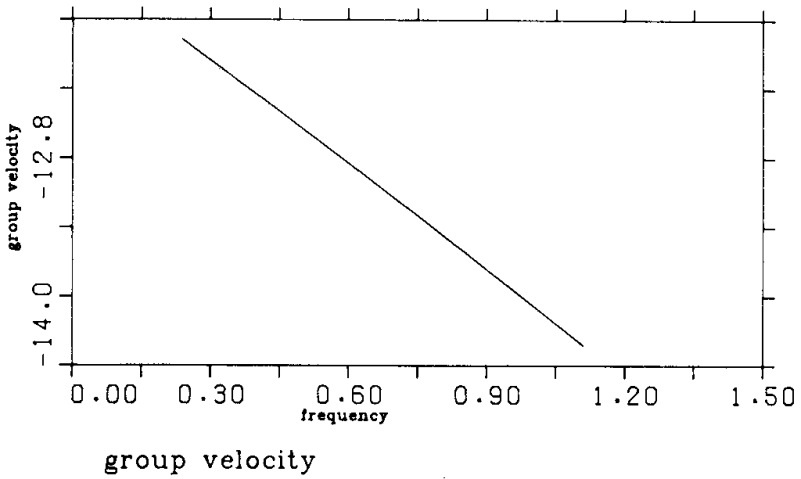

Figure 3(c) The group velocity/frequency curve obtained from the dispersion relation (4.22a).

first order corrections containing the wavenumber have been retained in (4.12), the dispersion relationship (4.22a) has been obtained by formally assuming $0<1-c\ll 1$. As such we have taken some "asymptotic freedom" in presenting results when c is not particularly "close" to one. In particular, the low non-zero phase speed cutoff obtained above is probably the result of the asymptotics and does not have any physical content.

The computed positive wavenumbers were found to lie in the relatively narrow interval $1.118<k<1.125$. The wavenumber is a

predominantly linear function of the frequency with a small super-linear correction (see Figure 3a). (Note that since k enters the dispersion relation as k^2 it follows $-k$ is also a solution. But since $c>0$ the frequency has the same sign as k, thus with no loss of generality k and ω are assumed positive.) The computed wavenumbers, which are slightly larger than one, imply that the along-front length scale (based on the inverse wavenumber) of the frontal-vorticity waves will be on the order of the e-folding shear of the geostrophic jet. Based on the length scale adopted in (3.12) a typical dimensional along-front wavelength is about $\lambda^* = 2\pi L/k \sim 58$ km.

In the Introduction it was suggested that the time scale associated with the warm–cold dipole pair in Figure 1 had to be small because the temperature signal was not observed in other XBT sections taken twelve hours before and after. This observation implies that the along-front (Döppler-shifted) group speed must be relatively large in order to account for the rapid passage of the signal. Figure 3c graphs the computed group velocities obtained from the dispersion relation. The group velocities are all large and negative, occurring in the interval $-13.8 < c_g < -12.1$, corresponding to a dimensional range of -2.8 m/s to -2.4 m/s. Consequently, although the wave phase is Döppler-shifted in the direction of the jet flow, the energy propagates in the opposite sense. This property is exactly analogous to *high* meridional wavenumber planetary Rossby wave propagation in a constant zonal flow. An estimate of a dimensional along-front time scale (T^*) is the length of time required for a Döppler-shifted wave packet to travel one wavelength, i.e., $T \sim \lambda^*/|c_g^* + U_*|$ which typically is about seven hours based on the above parameter values. Therefore, qualitatively, the neutral modes presented in this page are consistent with the interpretation of Figure 1 that the observed warm–cold core pair has short along-front time and space scales; but also, and importantly, the ageostrophic modes have lower frequencies and wavenumbers than the internal-gravity waves observed during *FRONTS'80* as speculated by Kunze (private communication, 1985).

The expansion coefficients a_n were found to approach zero as n increases extremely rapidly. For example, if $c=0.75$ the wavenumber was found to be 1.12 and (assuming $a_0=1$; a_0 will be left as the free amplitude constant) $a_2 = 8.5\times10^{-3}$, $a_4 = 3.7\times10^{-5}$ and $|a_n| < 10^{-7}$ for $n>6$. The a_n's were also always found to be non-negative.

Calculations for $\phi_1(\eta)$ were made using the first 20 evens terms in (4.15). Additional modes had absolutely no effect on the results to double precision accuracy.

The function $\phi_2(\eta)$ in (4.14c) will be the particular solution of the differential equation obtained by substituting (4.14c) into (4.12) (Drazin and Reid, 1981, Section 22) which can be written in the form

$$(\eta^2-1)\phi_{2_{\eta\eta}}-(\alpha+\beta\eta^2)\phi_2=-(\alpha+\beta)\{[(\eta^2-1)T]_\eta-\eta T\}, \quad (4.23)$$

where (4.15) has been used and

$$T(\eta)\equiv\sum_{n=0}^{\infty} a_n T_n^{(1)}(\eta). \quad (4.24)$$

It can easily be seen from (4.23) that

$$\phi_2(\pm 1)=\pm T(1) \quad (4.25)$$

because $T(\eta)$ is even about $\eta=0$. It will be shown in Section 5 that (4.25) implies that the wave-induced Reynolds stress discontinuity across the critical levels $\eta=+1$ and $\eta=-1$ are equal in magnitude but opposite in sign as required for two separable noninflectional critical levels (Drazin and Reid, 1981, Section 22). The implications of this property on the perturbation momentum flux and jet energetics will be discussed more completely in Section 5.

Because $\phi_2(\eta)$ is non-zero at the critical levels [cf. (4.25)], an expansion of the form (4.15) is inappropriate. It was found that the most convenient representation for $\phi_2(\eta)$ is in the form

$$\phi_2(\eta)=\sum_{n=0}^{\infty} b_n T_n^{(0)}(\eta), \quad (4.26)$$

where $T_n^{(0)}(\eta)$ are Gegenbauer polynomials with upper index zero [i.e. the Legendre polynomials, see (A.1)].

Substitution of (4.26) into (4.23) and rearranging the left and right-hand sides using the various identities in the Appendix results in the equation

$$\sum_{n=0}^{\infty} e_n T_n^{(1)}=(\alpha+\beta)\sum_{n=0}^{\infty} f_n T_n^{(1)}, \quad (4.27)$$

where e_n and f_n are given by, respectively,

$$\begin{aligned} e_n = {} & \beta n(n-1)[(2n+1)(2n-1)(2n-3)]^{-1} b_{n-2} \\ & + \{\beta(n+1)(n+3)[(2n+1)(2n+3)(2n+5)]^{-1} \\ & + \beta n(n+2)[(2n+1)^2(2n+3)]^{-1} + [\alpha - n(n-1)](2n+1)^{-1} \\ & - \beta n(n-1)[(2n-1)(2n+1)^2]^{-1}\} b_n \\ & + \{\beta(n+3)(n+4)[(2n+5)^2(2n+7)]^{-1} \\ & - \beta(n+1)(n+3)[(2n+3)(2n+5)^2]^{-1} \\ & - \beta n(n+2)[(2n+1)(2n+3)(2n+5)]^{-1} \\ & - [\alpha - (n+4)(n+3)](2n+5)^{-1}\} b_{n+2} \\ & - \beta(n+4)(n+3)[(2n+9)(2n+7)(2n+5)]^{-1} b_{n+4}, \end{aligned} \tag{4.28a}$$

$$f_n = n^2(2n+1)^{-1} a_{n-1} - (n+3)^2(2n+5) a_{n+1}. \tag{4.28b}$$

It follows from (4.27) that

$$e_n = (\alpha + \beta) f_n. \tag{4.29}$$

Note that since the odd a_n's are all zero, (4.29) implies that only odd f_n's, and consequently odd e_n's, are non-zero. Hence $\phi_2(\eta)$ will be an odd function about $\eta = 0$. Consequently, the contribution to the complete wave streamfunction $\phi(\eta)$ in (4.14c) from $\phi_2(\eta)$, and the product of $\phi_1(\eta)$ and the logarithmic term in (4.14c) will be odd about $\eta = 0$. However, the contribution to $\phi(\eta)$ from the product of $\phi_1(\eta)$ and the πi phase shift term in (4.14c) will be even about $\eta = 0$. It is this latter contribution which will be responsible for generating a constant northward Reynolds stress in the region in between the critical levels. Consequently $\phi(\eta)$ is neither even nor odd about $\eta = 0$ but is this *sum* of even and odd functions.

Equation (4.29) is an infinite dimensional inhomogeneous linear system from which b_n's are uniquely determined. Because of the

rapid convergence of the a_n's, the b_n's also rapidly converge. For example, in the case $c=0.75$ (again with $a_0=1$) $b_1=1.03$, $b_3=2.6\times10^{-2}$ and $b_5=1.7\times10^{-4}$. It was found that $|b_n|\leqq10^{-6}$ for $n\geqq7$. Calculations for $\phi_2(\eta)$ were made using the first 20 odd terms in (4.26). Additional Legendre polynomials had absolutely no effect on the results to double precision accuracy. It was found that the b_n's were always non-negative (because the a_n's were).

Under the approximation $y_c\ll1$ the leading order wave-induced perturbation in the mixed layer thickness (given by (3.21b) in the region $|y|<y_c$ is

$$h(\eta)\sim a_0\{1+r_0[2(1-c)/c]^{1/2}\eta\}\phi(\eta)+a_0r_0[c(1-c)/2]^{1/2}(1-\eta^2)\phi_\eta, \tag{4.31}$$

where a_0 is the free amplitude parameter.

Finally, the interior solutions (i.e. $|y|<y_c$) are patched to the exterior solutions (i.e. $|y|>y_c$) by requiring the reduced pressure $h(y)$ and normal velocity $\phi(y)$ to be continuous across $y=\pm y_c$ (Dickinson, 1968). It follows from (4.8) and (4.10a) that (Abramowitz and Stegun, 1970, Section 9.6)

$$\phi(y)\to A^+/(2\nu), \quad y\to y_c^+, \tag{4.32a}$$

$$\phi(y)\to A^-/(2\nu), \quad y\to -y_c^-. \tag{4.32b}$$

It also follows from (4.14), (4.15) and (4.25) that

$$\phi\to a_0T(1), \quad y\to y_c^-, \tag{4.33a}$$

$$\phi\to -a_0T(1), \quad y\to -y_c^+, \tag{4.33b}$$

where $T(1)$ is given by (4.24). Equations (4.32) and (4.33) imply

$$A^+=-A^-=2\nu T(1)a_0. \tag{4.34}$$

These conditions also ensure that the reduced pressure $h(y)$ is continuous at $y=|y_c|$ since in (3.21b) $(U_0-c)\phi_y\sim O[(y-y_c)\ln|y-y_c|]$ and $O[(y+y_c)\ln|y+y_c|]$ as $y\to y_c$ and $y\to -y_c$, respectively. There-

fore, in the limit as the critical levels are approached the ageostrophic contributions to the pressure field vanish and the continuity of the streamfunction implies the continuity of the pressure.

5. DISCUSSION AND APPLICATIONS

The energies of the vorticity wave solutions obtained in Section 4 is most conveniently described in terms of the wave-induced Reynolds stress. Following LeBlond and Mysak (1978, Section 41), the (non-dimensional) Reynolds stress in the along-front direction across a unit area in the transverse direction is given by

$$\tau = -\langle uv \rangle, \tag{5.1}$$

where u and v are the real along-front and transverse wave velocity components, respectively, and $\langle \cdot \rangle$ denotes an average over one wave cycle. Substitution of (3.17a) and (3.19a) into (5.1) yields

$$\tau = ik(\phi\phi_y^* - \phi^*\phi_y)/4, \tag{5.2a}$$

or equivalently

$$\tau = k\,\mathrm{Im}(\phi^*\phi_y)/2, \tag{5.2b}$$

where ϕ^* is the complex conjugate of ϕ and $\mathrm{Im}(\cdot)$ is the imaginary part of the argument. Note that in (5.2) ϕ refers to the *transverse* amplitude function [see (3.19a)] only.

In the regions $|y| > y_c$ ϕ is real, thus (5.2b) implies that

$$\tau \equiv 0 \quad \text{in} \quad |y| > y_c. \tag{5.3}$$

Alternatively, (5.3) can be concluded on account of the well-known constancy of the Reynolds stress for neutral solutions for the Rayleigh stability equation [except across non-inflectional critical levels; Drazin and Reid (1981, Section 22)], and the boundary conditions at infinity.

The Reynolds stress in $-y_c < y < y_c$ is constant but nonzero. Following the procedures described in Lindzen and Tung (1979),

(5.2b) is evaluated to be given by

$$\tau = k\pi(\alpha+\beta)|a_0|^2 W(\phi,\phi_1)/8, \tag{5.4}$$

where $W(\phi,\phi_1)$ is the Wronksian between the linearly independent solutions $\phi(\eta)$ and $\phi_1(\eta)$. The Wronksian is constant over the interval $-1<\eta<1$ and can be evaluated at $\eta=0$ to yield

$$W \equiv -\phi_\eta(0)\phi_1(0). \tag{5.5}$$

Substitution of (4.14a), (4.15) and (4.24) into (5.5) implies the interior critical-level Reynolds stress can be written in the form

$$\tau = k\pi(\alpha+\beta)|a_0|^2 T(0)[2\phi_{2\eta}(0)+(\alpha+\beta)T(0)]/16. \tag{5.6}$$

It turns out that, because the expansion coefficients a_n and b_n are non-negative and $T_n^{(m)}(0)>0$ when n is even [see (A.4) and the identities in Morse and Feshbach (1961, Chapter 6)], it follows from (5.6) that $\tau>0$ in $-1<\eta<1$ (i.e. $-y_c<y<y_c$). For example, if $c=0.75$, (5.6) is calculated to imply $\tau=2.29\ |a_0|^2$.

Defining $\Delta\tau(+y_c)$ and $\Delta\tau(-y_c)$ to be the jump as y increases in the Reynolds stress across the $y=+y_c$ and $y=-y_c$ critical levels, respectively, (5.3) implies that $\Delta\tau(+y_c)=-\tau$ and $\Delta\tau(-y_c)=+\tau$. Thus the sum $\Delta\tau(+y_c)+\Delta\tau(-y_c)\equiv 0$ as required for multiple non-inflectional critical levels (Drazin and Reid, 1981, Section 22).

The direction of wave energy propagation is determined by the sign of (LeBlond and Mysak, 1978, Section 41)

$$(U_0-c)\tau. \tag{5.7}$$

Since $U_0>c$ and $\tau>0$ in $-y_c<y<y_c$, it follows that the wave-induced energy flux is from the warm side of the front to the cool side. Thus the neutral vorticity wave extracts energy from the jet at the warm-side critical level and re-deposits it back into the jet at the cool-side critical level. Consequently, while there is no *net* energy transfer between the jet and the waves, the vorticity waves can lead to shear layers or asymmetries forming in the jet velocity profile in a neighborhood of the mean frontal axis. It is tempting to suggest that

as the shear layers form, $U'' \sim 0$ and the mechanism allowing the waves to propagate disappears.

Associated with the northward momentum flux is a northward heat flux. Thus the vorticity waves will act to tip the isotherms associated with NPSF back toward the horizontal (as in baroclinic instability).

In contrast to the situation in the critical-layer absorption of *internal-gravity* waves, the cross-front velocity associated with the frontal-vorticity wave does not vanish at the critical levels [this property is similar to that found in the theory for the critical-layer absorption of planetary Rossby waves; e.g. Dickinson (1968, 1970) and Lindzen and Rosenthal (1981)]. It follows from (3.17a) and (4.33) that

$$v(x, \pm y_c, t) = \mp kT(1)a_0 \sin(kx - \omega t). \tag{5.8}$$

The wave-induced along-front velocities are logarithmically singular across the critical levels (see Figure 8). It easily follows from (3.17a), (4.5) and (4.14a) that

$$u \equiv -\phi_y \sim -2a_0 T(1) y_c^{-1} \ln|y - y_c| \cos(kx - \omega t) \tag{5.9}$$

as $y \to +y_c$. The behaviour at $y = -y_c$ is similar. The along-front logarithmically singular velocity at the critical levels is, of course, unphysical and underlines the fact that at the critical levels the simple linear model considered here must be modified to include other physics, e.g. viscosity or non-linearity.

The remaining qualitative features of the absorbed vorticity waves is conveniently described using transverse sections of the solution, and horizontal contour plots. Figure 4a is a plot of a transverse section of the wave streamfunction [given by (4.14a) in $|y| < y_c$ and the leading order solution ϕ obtained in Section 4.1 for $|y| > y_c$] evaluated for $c = 0.75$. In Figures 4 and 5 the phase $kx - \omega t = 0$. The free multiplicative constant a_0 is chosen to be 0.81 so that the maximum and minimum of $\phi(y)$ is about $+1$ and -1, respectively, along the zero phase line. Figure 4b is a transverse section plot of the total wave plus jet streamfunction. The jet is geostrophic so the thickness perturbation associated with the jet is also the jet streamfunction, see (3.16). The jet streamfunction is shown in Figure 7a.

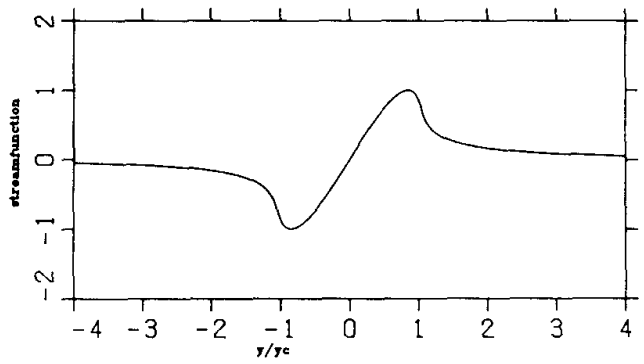

Figure 4(a) Transverse section of the wave streamfunction taken along the phase $kx-\omega t=0$. The free amplitude constant $a_0=0.81$ so that the maximum and minimum amplitude is about 1.0 and -1.0, respectively.

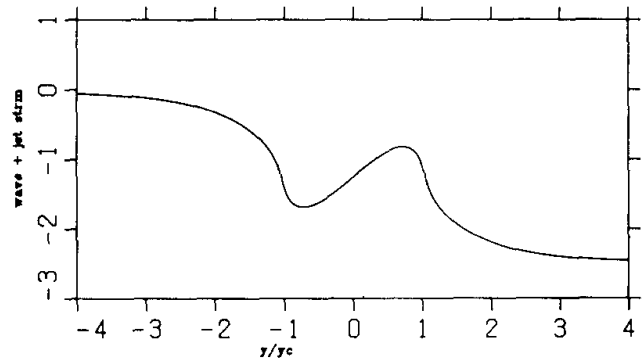

Figure 4(b) Transverse section of the wave plus jet streamfunction. The phase and amplitude constant are as in Figure 4(a).

Figures 5a and 5b depict transverse sections of the thickness perturbation associated with the absorbed vorticity wave and the sum of the jet and wave thickness, respectively. The wave thickness anomaly, given by (3.20b), is composed of the $O(1)$ geostrophic component (Figure 4a) and the $O(r_0)$ ageostrophic terms. The principal effect of the ageostrophic terms will be to shift the wave streamfunction "upwards" and consequently to force the node in the total wave thickness anomaly toward the "warm" side of the front. Kunze and Sanford (1984) remarked that the XBT section shown in Figure 1 possessed this property.

One of the reasons for working with the perturbation mixed-layer

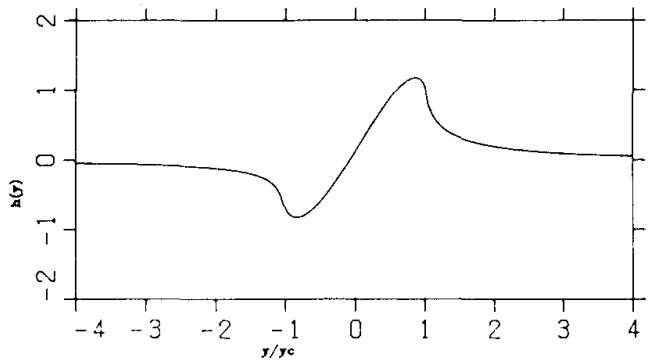

Figure 5(a) Transverse section of the wave mixed layer thickness anomaly (which is positively correlated to the temperature anomaly) given by (3.20b). The ageostrophic terms act to increase (decrease) the cool (warm) side anomaly and shift the node toward the warm side. The phase and amplitude constant are as in Figure 4.

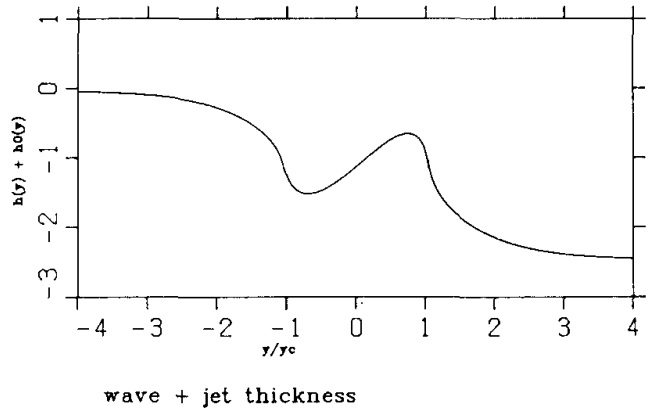

Figure 5(b) Transverse section of the total wave plus jet mixed layer thickness anomaly. The phase and amplitude constant are as in Figure 4.

thickness as a dynamical variable, rather than the deflection in the base of the mixed layer, was that the thickness is positively correlated with temperature anomalies. Note the striking similarities between the total wave plus jet thickness perturbation, shown in Figure 5b, and the XBT temperature section shown in Figure 1. By increasing or decreasing a_0 the absolute amplitudes of the wave-related extrema in Figure 5b would increase or decrease, respectively.

The effect of the neutral wave perturbation on the along-front jet structure is depicted in Figures 7 and 8. The warm (cool) side of the front corresponds to the lower (upper) horizontal axis. In both

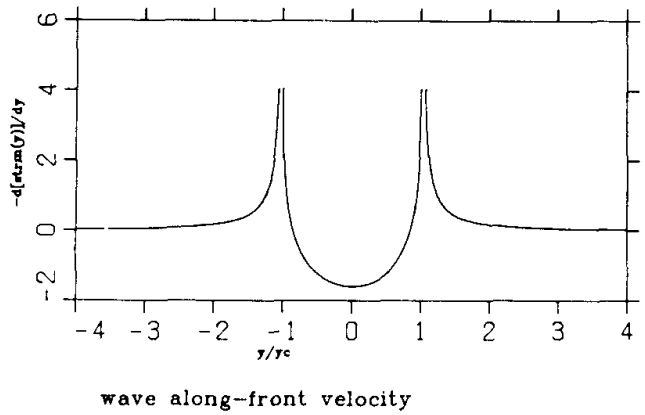

Figure 6 Transverse section of the along-front vorticity as given by (3.17a). At the critical levels the along-front velocity is logarithmically singular. The phase and amplitude constant are as in Figure 4.

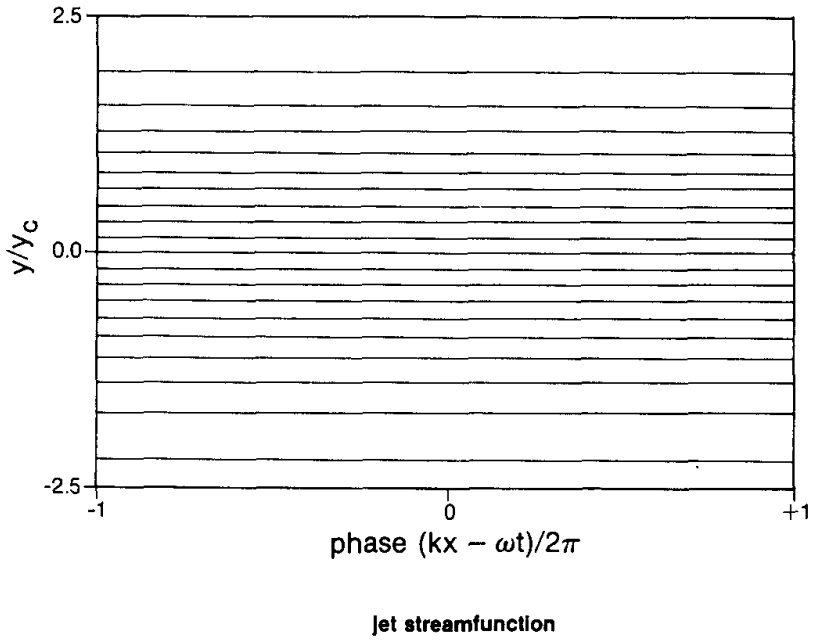

Figure 7(a) Contour plot of the jet streamfunction. The contour intervals are ± 0.13.

Figure 7 and 8, the vertical and horizontal axis scalings are the same (see Figure 7a). The unperturbed jet streamfunction is shown in Figure 7a. The wave streamfunction is shown in Figure 7b. The maximum and minimum wave streamfunction values are about $+1.0$ and -1.0 (because of the choice of $a_0 = 0.81$) and the contour interval is about ± 0.1. The plus and minus signs in Figure 7b

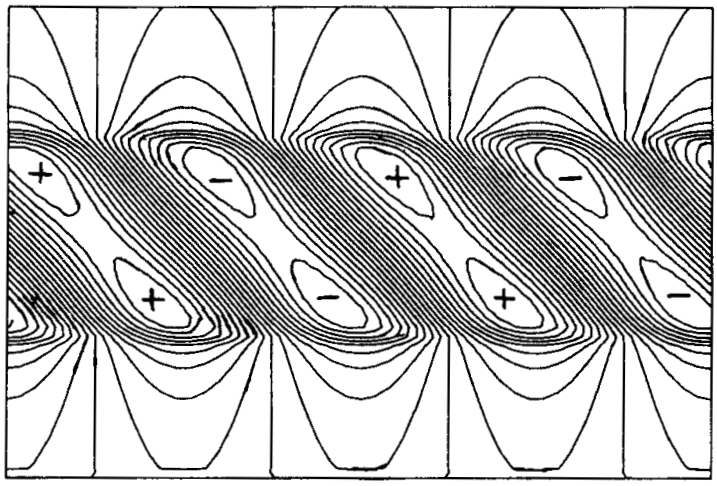

Figure 7(b) Contour plot of the wave streamfunction showing the horizontally tilted "cat's eyes" doublets. The maximum and minimum values are 1.0 and -1.0, respectively, and the contour interval is about ± 0.1. The amplitude constant is as given in Figure 4.

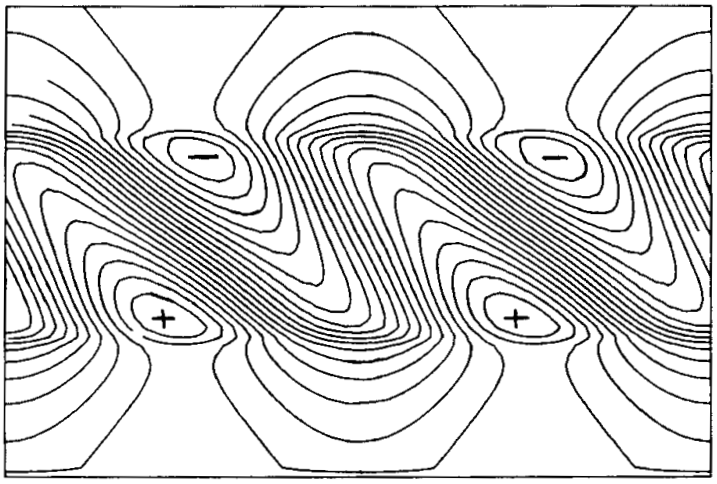

Figure 7(c) Contour plot of the wave plus jet streamfunction. The maximum and minimum values are about 0.4 and -2.9, respectively, and the contour interval is about ± 0.2. The amplitude constant is as given in Figure 4.

indicate the locations of maximum and minimum streamfunction values, respectively. Thus the flow is anti-cyclonic around the plus

signs and cyclonic around the minus signs. Figure 7c depicts the total wave plus jet streamfunction. The maximum and minimum values in Figure 7c are approximately 0.4 and -2.9, respectively ($a_0 = 0.81$ in all the counter plots), and the contour interval is about ± 0.2. The jet is perturbed into a distorted meander pattern. The ridges and troughs propagate toward the *east* but the group velocity is directed toward the *west*. The ridges are associated with the positive streamfunction anomaly and the troughs with the negative streamfunction anomaly. Figures 4a, b and 5a, b correspond to a transverse section taken along $kx - \omega t = 2n\pi$ ($n = 0, 1, 2, \ldots$) in Figures 7b, c and 8a, b, respectively. The horizontal "westward" phase tilt seen in Figures 7 and 8 is the result of the π phase shift found in the solutions in the region between the critical levels. Alternatively, the westward phase shift is the result of the "northward" heat and momentum transport averaged over one wave cycle.

Figure 8a and 8b illustrate the thickness (or temperature) anomaly associated with the wave and wave plus jet situation, respectively. The mixed layer thickness anomaly is principally determined by the streamfunction [the geostrophic contribution in (3.17b)], but does contain a non-negligible $O(r_0)$ ageostrophic component. As shown qualitatively by comparing Figure 8a with Figure 7b, the ageostrophic terms act to amplify the temperature anomaly on the cool side of the jet and diminish the temperature anomaly on the warm side. The maximum and minimum values in the wave-induced thickness anomaly are about 1.22 and -1.20, respectively. ($a_0 = 0.81$) and the contour interval in Figure 8a is ± 0.21. The maximum and minimum in Figure 8b, which depicts the total wave plus jet thickness anomaly, is 0.22 and -3.1, respectively, and the contour interval is ± 0.17.

A detailed comparison between the theory developed in this paper and the anomalous XBT section shown in Figure 1 is unwarranted because the data represents a single isolated observation and a detailed time series describing the along-front evolution of the warm–cold temperature pair is not available. Also, it is very unlikely that the signal shown in Figure 1 is simply a single wave mode and is more likely a superposition of many allowed wave modes. However, there are several general properties of the theory developed in this paper which agree with the qualitative interpretation given to the event shown in Figure 1.

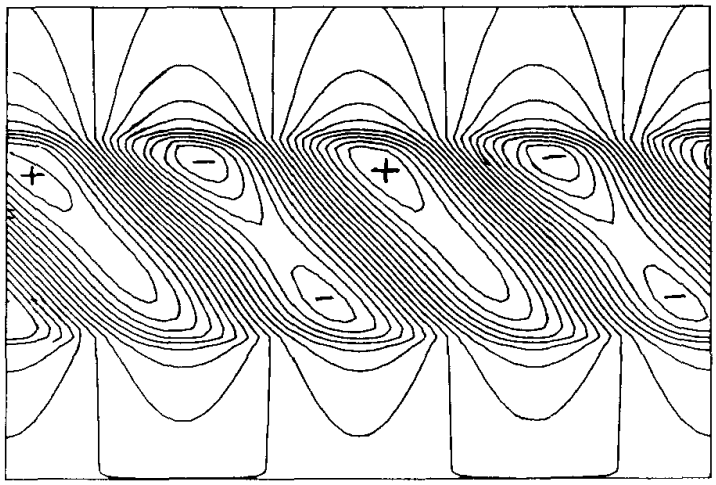

Figure 8(a) Contour plot of the wave mixed layer thickness (temperature) anomaly. The maximum and minimum values are 1.22 and 1.20, respectively, and the contour interval is about ± 0.21. The amplitude constant is as given in Figure 4.

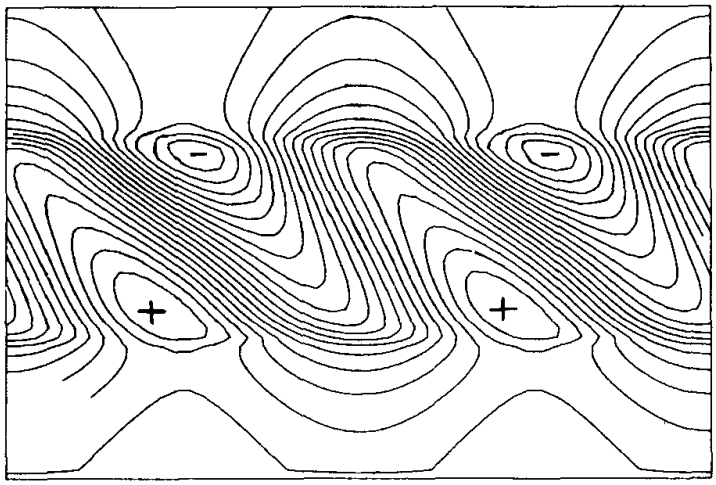

Figure 8(b) Contour plot of the wave plus jet mixed layer thickness (temperature) anomaly. The maximum and minimum values are 0.22 and -3.1, respectively, and the contour interval is about ± 0.17. The amplitude constant is as given in Figure 4.

For example, there is the obvious dominant odd-like symmetry in the wave plus jet transverse thickness section shown in Figure 5b and Figure 1. [It was shown in Section 4, $\phi(\eta)$ is the sum of odd and even terms.] Kunze and Sanford (1984) pointed out that the "node"

in the temperature dipole in Figure 1 was displaced toward the warm side of the front. It has been shown in this paper that this can be accounted for by the ageostrophic contribution to the total wave-induced temperature anomaly. Because the temperature dipole was not seen in another temperature section taken twelve hours later, Kunze (private communication, 1985) inferred that the signal must have had short along-front time and length scales. The theory presented here predicts an along-front wavelength of about 58 km and an along-front inviscid group velocity on the order of 2 m/s (retrograde with respect to the jet). The estimate computed for an along-front time scale based on the wavelength and Döppler-shifted group velocity was about seven hours. Therefore, the general properties of the solution obtained above agrees, at least qualitatively, with the interpretation given to Figure 1 as described in the Introduction.

6. SUMMARY

A theory has been presented which describes the along-front propagation and cross-front trapping, due to the presence of symmetric critical levels, of ageostrophic nondivergent perturbations of geostrophic jets. The perturbations are dispersive neutral vorticity waves which use the continuous jet vorticity gradient as a pseuso-β effect.

The wave streamfunction and associated temperature anomaly have the appearance (see Figures 7 and 8) of tilted "cat's eyes doublets" (in the amplitude limit) which propagate in the direction of jet flow, but which have relatively large retrograde group velocities. The phase shift in the wave field across the critical levels resulted in an averaged momentum and heat transfer from the warm to the cool side of the jet. There is, however, no *net* wave-mean flow energy exchange.

An analytical solution describing the wave streamfunction between the critical levels was obtained under the approximation that the distance from the jet axis to the critical levels was small compared to the *e*-folding shear of the jet. With this approximation, the Rayleigh stability equation (describing the transverse structure in the wave field) was to leading order, a generalized spheroidal wave equation. The equation retained the essential physics: namely, the appearance of symmetrically placed critical levels and a relatively constant jet

vorticity gradient. A solution to this equation was found by a spectral expansion in terms of Gegenbauer polynomials. The derivation of the dispersion relation can be viewed as resulting from the requirement that the wave field had a removable logarithmic singularity at the critical levels. The allowed wave streamfunctions were single-node functions with respect to the frontal axis of symmetry. The effect of the ageostrophic terms was to shift the "node" in the wave temperature field toward the warm side of the front.

The nondimensional frequencies obtained from the dispersion relationship were found to lie in the range (0.2, 1.2) corresponding to a dimensional period range of about (3.0, 21.0) days. The nondimensional wavenumber range obtained from the dispersion relationship was found to be relatively narrow (1.118, 1.125) corresponding to a dimensional along-front wavelength of about 58 km. The computed group velocities were all retrograde and had relatively large magnitudes in comarison to the phase speeds. Typical inviscid dimensional group velocities were found to be on the order of -2.5 m/s. An estimate of a dimensional along-front time scale (T^*) is the type required for a Döppler-shifted wave packet to travel one wavelength. The above numbers imply $T^* \sim 7$ hours.

The solutions exterior to the critical levels was obtained by asymptotically matching the leading order singular behaviour of the streamfunction exterior to the critical levels to a WKB solution valid far from the critical levels.

The development of the above theory was motivated by the observation of an anomalous XBT temperature section observed during the *FRONTS'80* experimental program. Figure 1 was briefly commented on but not published in Kunze and Sanford (1984). The principal distinguishing characteristics associated with Figure 1 are: the single-node odd-like symmetry of the perturbation temperature field, the displacement to the warm side of the front of the temperature dipole, a rapid along-front time scale since the feature in Figure 1 was not seen 12 hours later in another XBT section, and the cross-front length scale deduced from Figure 1 which suggest that the feature was "too long" to be interpreted as an internal-gravity wave, but had scales smaller than the deformation radius for the region [about 37 km, Emery *et al.* (1984)]. The latter observation suggested that horizontal mass divergences could be ignored and attention could be focused on a vorticity wave interpretation.

The theory presented is able to qualitatively reproduced the above observations. Still, many other interpretations of Figure 1 are possible and were discussed in the Introduction. Also, many other influences have been neglected in the simple theory presented here. A realistic modeling of the actual baroclinicity of the NPSF has been reduced to its simplest form, a reduced-gravity model. The role of nonlinearity and viscosity which is important in the long term evolution of critical-layer absorbed vorticity waves (Benny and Bergeron, 1969; Maslowe, 1985; Warn and Warn, 1978) has been ignored here.

Acknowledgements

The author would like to thank Dr Eric Kunze for showing him Figure 1 and for initial discussions on its interpretation. The author also thanks Dr Kunze and Prof. Lawrence A. Mysak for reading a draft of this manuscript and making many helpful comments. This work was initiated while the author was a post-doctoral fellow supported by National Science Foundation grants awarded to Professor Glenn R. Flierl of M.I.T. Final preparation of the manuscript was supported by operating research grants from the University of Alberta Central Research Fund, the Natural Sciences and Engineering Research Council of Canada, and the Atmospheric Environment Service of Canada.

References

Abramowitz, M. and Stegun, I. A., *Handbook of Mathematical Functions*, Dover Press (1972).

Bender, M. L. and Orszag, S. A., *Advanced Mathematical Methods for Scientists and Engineers*, McGraw-Hill (1978).

Benny, D. J. and Bergeron, R. F., "A new class of nonlinear waves in parallel flows," *Stud. Appl. Math.* **48**, 181–204 (1969).

Boyce, B. E. and DiPrima, R. C., *Elementary Differential Equations and Boundary-value Problems*, Wiley, New York (1977).

Clarke, J. H. E., "The theory of the vertical propagation of quasi-geostrophic disturbances in the presence of distorted background flows," *J. Atmos. Sci.* **32**, 2217–2228 (1975).

Dickinson, R.E., "On the exact and approximate linear theory of vertically propagating planetary rossby waves forced at a spherical lower boundary," *Mon. Wea. Rev.* **96**, 405–415 (1968a).

Dickinson, R. E., "Planetary rossby waves propagating vertically through weak westerly wind wave guides," *J. Atmos. Sci.* **25**, 984–1002 (1986b).

Dickinson, R. E., "Development of a Rossby wave critical level," *J. Atmos. Sci.* **27**, 627–633 (1970).

Drazin, P. G. and Howard, L. N., "Hydrodynamic stability of parallel flow of inviscid fluid," in *Advances in Applied Mechanics* **9**, 1–89, Academic Press, New York (1966).

Drazin, P. G. and Reid, W. H., *Hydrodynamic Stability*, Cambridge University Press (1981).

Duffy, D. G., "The barotropic instability of Rossby wave motion: a re-examination," *J. Atmos. Sci.* **32**, 1271–1277 (1975).

Emery, W. J., Lee, W. G. and Magaard, L., "Geographic distributions of density, Brunt-Väisälä frequency and Rossby radii in the North Pacific and North Atlantic," *J. Phys. Oceanogr.* **14**, 294–317 (1984).

EOS Transactions, *Upper Ocean Fronts Abstracts, AGU* **61** (46), 1000–1002 (1980).

Gill, A. E., "The stability of planetary waves on an infinite Beta-plane," *Geophys. & Astrophy. Fluid. Dyn.* **6**, 26–47 (1974).

Killworth, P. D., "Long-wave instability of an isolated front," *Geophys. & Astrophys. Fluid Dyn.* **25**, 235–258 (1983).

Kunze, E. and Sanford, T. B., "Observations of near-inertial waves in a front," *J. Phys. Oceanogr.* **14**, 566–581 (1984).

LeBlond, P. H. and Mysak, L. A., *Waves in the Ocean*, Elsevier (1978).

Lindzen, R. S., Farrell, B. and Tung, K. K., "The concept of wave overreflection and its application to baroclinic instability," *J. Atmos. Sci.* **37**, 44–63 (1980).

Lindzen, R. S. and Rosenthal, A. J., "A WKB asymptotic analysis of baroclinic instability," *J. Atmos. Sci.* **38**, 619–629 (1981).

Lindzen, R. S. and Tung, K. K., "Wave overreflection and shear instabilities," *J. Atmos. Sci.* **35**, 1626–1632 (1978).

Lipps, F. B., "The barotropic stability of the mean winds in the atmosphere," *J. Fluid Mech.* **12**, 397–407 (1962).

Lipps, F. B., "Stability of jets in a divergent barotropic fluid," *J. Atmos. Sci.* **20**, 120–129 (1963).

Lorenz, E. N., "Barotropic instability of Rossby wave motion," *J. Atmos. Sci.* **29**, 258–264 (1972).

Maslowe, S. A., "Shear flow instabilities and transition," in *Hydrodynamic Instabilities and the Transition to Turbulence*, Topics in Applied Physics, **45** (2nd edition), 181–228, Springer-Verlag (1985).

Mayer, D. A., Hansen, D. V. and Ortman, D. A., "Long-term current and temperature observations on the middle Atlantic shelf," *J. Geophys. Res.* **84**, 1776–1792 (1979).

Milne-Thompson, L. M., *The Calculus of Finite Differences*, Macmillan (1933).

Morse, P. M. and Feshbach, H., *Methods of Theoretical Physics*, McGraw-Hill (1961).

Niehaus, M. C. W., "Instability of non-zonal baroclinic flows," *J. Atmos. Sci.* **37**, 1447–1463 (1980).

Niiler, P. P., "*FRONTS-80*—a study of the North Pacific Subtropical Front," *Nav. Res. Rev.* **34**, 41–50 (1982).

Paldor, N., "Linear stability and stable modes of geostrophic fronts," *Geophys. & Astrophys. Fluid Dyn.* **24**, 299–326 (1983).

Pedlosky, J., *Geophysical Fluid Dynamics* (2nd ed.), Springer-Verlag (1987).

Roden, G. I., "Mesoscale thermohaline, sound velocity and baroclinic flow structure of Pacific Subtropical Front during the winter of 1980," *J. Phys. Oceanogr.* **11**, 658–675 (1981).

Roden, G. I. and Paskauski, D. F., "Estimates of rates of frontogenesis and frontolysis in the North Pacific Ocean using satellite and surface meteorogical data from January 1977," *J. Geophys. Res.* **83**, 4545–4550 (1978).

Savic, P., "On acoustically effective vortex motion in gaseous jets," *Philos. Mag.* **32** (7), 245–252 (1941).

Stern, M. E., "The stability of thermoclinic jets," *Tellus* **13**, 503–508 (1961).

Stern, M. E., "Interaction of inertia-gravity waves with the wind," *J. Mar. Res.* **35** (3), 479–498 (1977).

Tung, K. K., "On the convergence of spectral series—A reexamination of the theory of wave propagation in distorted background flows," *J. Atmos. Sci.* **33**, 1816–1820 (1976).

Van Woert, M., "The subtropical front: Satellite observations during *FRONTS'80*," *J. Geophys. Res.* **87**, 9523–9536 (1982).

Warn, T. and Warn, H., "The evolution of a nonlinear critical level," *Stud. Appl. Math.* **59**, 37–71 (1978).

Appendix

Here, a list of the relevant properties of Gegenbauer polynomials required in this study are presented for the convenience of the reader. For a complete description see Morse and Feshbach (1961, Sections 5.2 and 6.3) or Abramowitz and Stegun (1970, Chapter 22).

The Gegenbauer polynomial $T_n^{(m)}(\eta)$ (m and n are non-negative integers) satisfies the differential equation

$$[(\eta^2-1)(d^2/d\eta^2)+2(m+1)\eta(d/d\eta)-n(n+2m+1)]T_n^{(m)}=0. \quad \text{(A.1)}$$

When $m=0$, $T_n^{(0)}(\eta)$ are the *Legendre* polynomials.

The recurrence formulas used in this study are:

$$(2m+2n+1)\eta T_n^{(m)}=(n+1)T_{n+1}^{(m)}+(2m+n)T_{n-1}^{(m)}, \quad \text{(A.2)}$$

$$(2m+2n+1)T_n^{(m)}=T_n^{(m+1)}-T_{n-2}^{(m+1)}, \quad \text{(A.3)}$$

$$dT_n^{(m)}/d\eta=T_{n-1}^{(m+1)}, \quad \text{(A.4)}$$

$$d[(\eta^2-1)^m T_n^{(m)}]/d\eta=(n+1)(n+2m)(\eta^2-1)^{m-1}T_{n+1}^{m-1}. \quad \text{(A.5)}$$

In this study only upper index $m=0$ and $m=1$ are required. It is useful to note $T_0^{(0)}(\eta)=T_0^{(1)}(\eta)=1$, $T_1^{(0)}(\eta)=\eta$ and $T_1^{(1)}(\eta)=3\eta$ upon which the remaining $n\geqq 2$ polynomials can be constructed [cf. (A.2)].